IEEE Access
Multidisciplinary | Rapid Review | Open Access Journal

Received 20 April 2023, accepted 9 June 2023, date of publication 10 July 2023, date of current version 27 July 2023.

Digital Object Identifier 10.1109/ACCESS.2023.3293735

RESEARCH ARTICLE

Multiple Tissue Sample Collection Device for MRI Guided Transrectal Prostate Biopsy: Optimization and MRI Compatibility Tests

FARRUKH ANIQUE[1], RONGRONG LIU[1], MUHAMMAD UMAR FAROOQ[1], SUNG SUK OH[2], JUNG KI JO[3], AND SEONG YOUNG KO[1], (Member, IEEE)

[1]Department of Mechanical Engineering, Chonnam National University, Gwangju 61186, Republic of Korea
[2]Medical Device Development Center, Daegu–Gyeongbuk Medical Innovation Foundation (K-MEDI Hub), Daegu 41061, Republic of Korea
[3]Department of Urology, Hanyang University College of Medicine, Seoul 04763, Republic of Korea

Corresponding author: Seong Young Ko (sko@jnu.ac.kr)

This work was supported in part by the Korea Medical Development Fund Granted by the Korea Government (the Ministry of Science and ICT; the Ministry of Trade, Industry and Energy; the Ministry of Health and Welfare; and the Ministry of Food and Drug Safety) under Grant KMDF_PR_20200901_0122 and Grant 1711138226; and in part by the Chonnam National University under Grant 2018-3528.

ABSTRACT Biopsies are one of the most common ways to diagnose and make a prognosis of prostate cancer. Transrectal and Transperineal approaches are used to access the prostate for biopsy. Advancements in Magnetic Resonance Imaging (MRI) offer a clear visualization of soft tissues and improved volumetric clarity. Real time MRI guidance can significantly change the paradigm of soft tissue biopsy. Proposed is a device with the ability to collect the tissue samples taken by a biopsy needle during an MRI guided Prostate biopsy and store them temporarily. This could help avoid interruption during the process and make the entire process teleoperated. The proposed design consists of a double layer of paper, rolling over a set of pulleys. Paper collects and stores the core tissue sample. Experiments have been performed to optimize paper tension, speed, and size. Tissue collection performance improvement is noticed with optimum paper tension, speed, and size. A test has also been performed in an MRI environment to check MR compatibility of the device. The device is MRI conditional and demonstrates a maximum of 13.1% SNR reduction in MR images. The proposed device exhibits the potential to be integrated with an MRI safe or conditional robotic manipulator for real time MRI guided Prostate biopsy.

INDEX TERMS Magnetic resonance imaging (MRI), multiple tissue sample collection device (MTSCD), prostate biopsy, teleoperation, transrectal.

I. INTRODUCTION

Cancer is the first or second leading causes of death before the age of 70 in 112 countries. It has claimed 9.9 million lives in 2020 alone. Prostate cancer is the second most diagnosed cancer in men in 183 countries with 375,000 mortalities in 2020 [1]. Digital rectal examination (DRE) or a prostate specific antigen (PSA) test could be one of the very first indicators of Prostate cancer. PSA screening with or without DRE is recommended for men with a family member diagnosed with Prostate cancer [2]. Conventionally, men having a PSA level of 4.0ng/mL or higher have been recommended to have a further evaluation [2]. PSA has been shown to detect a significant number of tumors missed by DRE [3]. Gleason Score assigned to suspected tissue samples, after a laboratory analysis, is considered to be the best predictor of aggressiveness of tumor [4]. It has 5 grade groups, group 1 being associated with the lowest risk and group 5 being the highest risk of cancer [5]. Prostate biopsy is performed to provide a tissue sample for laboratory analysis. Prostatic biopsy is considered after having abnormal results of PSA and/or DRE even if no abnormality is observed during transrectal ultrasonography [3]. Over two million prostate biopsies are performed each year worldwide.

The associate editor coordinating the review of this manuscript and approving it for publication was Jingang Jiang.

Transrectal ultrasound (TRUS) guided biopsy is the most popular technique in the world for prostate biopsy due to its simplicity and requirement of local anesthesia [6], [7]. Classically, TRUS guided biopsies are systematic and multiple core samples are collected from different sections of the prostate. In some studies, this method has shown possible undesired outcomes including unnecessary biopsies, false negatives, limited ability to sample in the anterior part of the prostate [8], overestimation or underestimation of the Gleason score [9], lower detection rate of clinically significant cancers [4]. In recent years, research motives have been diverted significantly toward targeted biopsies [10]. Systematic biopsies have been proved to result in a lower detection rate of clinically significant cancers when compared with targeted biopsies [7]. To improve the detection rate, an increased number of systematic biopsies can be performed but it comes with the disadvantage of adverse effects like bleeding and transient urinary retention [10].

With the advancements in the field of MRI, we now have MRI systems with improved soft tissue contrast and enhanced spatial clarity. This gives us an opportunity to use this imaging modality to scan and target the region of interest in the gland before performing the biopsy. High resolution T-2 weighted MR images have shown a potential of detecting cancer in the transition zone of the Prostate. Diffusion Weighted Imaging (DWI) is based on the Brownian motion of water molecules. Dynamic Contrast Enhanced Imaging (DCEI) and MR Spectroscopic Imaging (MRSI) utilize perfusion characteristics and metabolic profiles respectively. A blend of DWI, DCEI and MRSI imaging techniques is called multi parametric MRI (mpMRI). Multiparametric MRI (mpMRI) targeted biopsy has yielded a better detection of clinically significant cancers [4], [11]. MRI coordinated risk categorization helps to target the most aggressive lesions and results in significantly improved detection over TRUS guided biopsies [12], [13], [14]. However, in some cases targeted biopsy may result in a lower Gleason score when compared with the systematic biopsy [15]. Advanced multiparametric MR imaging modes such as T2-weighted anatomical dynamic contrast-enhanced imaging, proton magnetic resonance spectroscopic imaging and DWI have immensely improved imaging results [16], [17].

With these developments in the field of MRI, studies are being conducted now to use MRI to detect and localize the cancer regions in prostate prior to performing the biopsy. TRUS-guided approach provides the localization of the prostate while MRI can actually locate the suspected regions within it [4]. Turkbey et al. stated that mpMRI is the best imaging modality for the detection of prostate cancer [18]. In some studies patients with negative results after TRUS biopsies were later found to have tumors in the anterior zone of prostate [4]. Engehausen et al. conducted a study of 96 men who underwent real-time MRI guided biopsies. Prostate cancer was detected in 39 of 96 men and the rate of missed cancer was demonstrated to be at most 10.4%. A pathological analysis of prostate specimens of 31 patients, who underwent radical prostatectomy, revealed the sensitivity of MRI guided biopsy to be 95.8% [19]. Moore et al. concluded after a systematic literature review that MRI guided biopsy had a rate of detection of significant cancer equivalent to TRUS biopsy, however because of effective localization of suspected region, the former approach required fewer biopsies and had a lower rate of detection of insignificant cancer [20]. Several studies have been done demonstrating a superior detection rate of MRI guided biopsy over the traditional approach [21], [22], [23], [24], [25], [26]. However, a qualified and profoundly skilled reader is required to analyze the MRI scan and it has been shown that a less experienced reader can miss significant tumor detection [27]. A blend of both MR and US imaging modalities has also been introduced, where pre-scanned MR images are fused with real time US images. MR images give indications which zones are the most critical to target. This procedure results in detection of more significant cancers. It requires a fusion software to fuse and process the images from both scans [4].

A teleoperated robotic system for real-time MRI-guided prostate biopsy is under development in our research consortium. The system will include three major modules; an automatic loading biopsy gun device for multiple sampling, a multiple tissue sample collection and storage device, and a 6-degree-of-freedom (6-DOF) manipulator to position and orient the aforementioned modules. In this paper, a detailed description about the multiple tissue sample collection device will be provided.

This paper is organized into six sections. The first section concludes with this paragraph. The second section discusses a literature review related to the work presented in this paper. The third and fourth sections explain the design, and preliminary performance evaluation and optimization experiments conducted, respectively. The fifth and sixth sections contain concluding remarks and future plans regarding the work presented in this paper.

II. LITERATURE REVIEW

To make the MRI-guided biopsy procedure fully automatic and teleoperated, various challenges are there to be solved. To manipulate and position the biopsy needle in three-dimensional (3D) space is the most important of these. Several research teams have been working on it and numerous robotic systems have been developed [28].

MR imaging technique requires a special environment with an absolute absence of magnetic materials. This creates a constraint over the materials of robot parts, motors, and other accessories to be used in the system. The US Food and Drug Administration has defined the materials posing no known hazard in MRI environments as ''MRI Safe'' and materials posing known hazards as ''MRI Unsafe''. Another term ''MRI Conditional'' means that the device is MRI safe under certain conditions and does not affect the scanner function or be affected by the MR system less than the desired extent [29].

Elayaperumal et al. designed a five degrees of freedom (5-DOF) passive parallel mechanism with a master and slave platform for MR imaging guided interventions. It combines two parallel mechanisms and allows the physician to control and manipulate the needle by moving the gimbal installed on the master platform while standing away from the patient in the proximal direction [30]. Mendoza et al. demonstrated a 3-DOF master-slave based testbed for MRI-guided biopsy. A novel piston-cylinder based actuator at the master end was connected to a similar unit at the slave end with a pneumatic line [31]. Chen et al. presented a design of CoreXY-based system for focal laser ablation in prostate with two active DOF using piezoelectric motors and one passive rotational DOF [32]. Sang et al. proposed a 4-DOF, parallel-type pneumatically actuated robotic system for Transperineal prostate biopsy and brachytherapy. It utilizes belt and pulley mechanism to transmit the torque from a pneumatic actuator to the robotic system [33], [34]. Stoianovici et al. developed an MRI-safe pneumatic motor called ''PneuStep'' which is capable of supplying discrete rotary movement and is operated by pulsed pressure waves generated by a pneumatic distributor [35]. The same team introduced a Transperineal prostate biopsy robotic system based on PneuStep motor actuation developed earlier. The system is parallel type and has 5-DOF [36]. Jiang et al. developed a 5-DOF pneumatic-piezoelectric hybrid-driven MR compatible robot for prostate interventions, using a serial-parallel hybrid mechanism [37]. Lin et al. demonstrated a 6-DOF robot which uses piezoelectric actuation. Three DOFs are for cartesian module, two DOFs are for the orientation module and one DOF is for needle insertion module [38]. Su et al. designed a 6-DOF piezoelectric actuated robotics system for MRI-guided prostate percutaneous therapy. It has a 3-DOF needle driver module and 3-DOF cartesian motion module [39]. Moreira et al. presented a novel 9-DOF design for MRI guided prostate biopsy. Design is based on a piezoelectric based linear actuator and uses pneumatic actuation for needle operation [40]. Some of these systems are biopsy specific where others are for general percutaneous intervention in the prostate gland.

To the best of our knowledge, all of these systems lack a system to collect and store the transected tissue sample. Once the needle has been operated and transected the tissue sample from the gland, a staff member needs to collect the core sample from the needle before it takes another sample. This step hinders the complete teleoperation of MRI guided prostate biopsy. After every core sample collection, a staff member needs to interrupt the biopsy process to collect and store the sample. The automation of this step can not only automate the whole biopsy process but also can decrease the process time significantly. Hibner and Ludzack have a patent for a biopsy device in various countries [41]. This device has discrete tissue chambers with small openings at the bottom. After acquiring the core sample, the needle is brought in this chamber and a vacuum pressure is applied to the openings

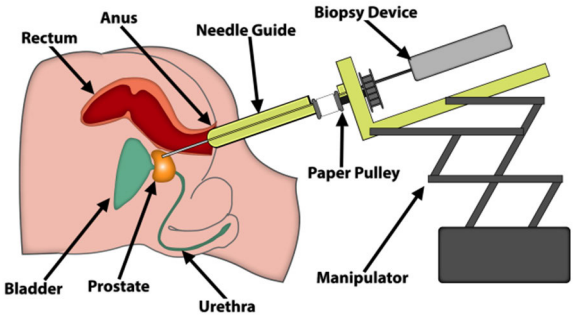

FIGURE 1. Schematic configuration of the proposed device integrated with manipulator and biopsy device during transrectal prostate biopsy.

at the bottom of the chamber which sucks the sample out of the needle and into the chamber. This device requires vacuum pressure and is complex in its structure. Anderson et al. have a patent for a device for cutting and collecting soft tissue from breast [42]. This device has a membrane which receives the sample from a sharp thin cutting structure and stores inside it. This device is not feasible to be used for prostate biopsy. Pesce et al. have a patent for tissue extraction and collection device in multiple countries [43]. This device uses a rotating tool to extract and collect tissue samples for grafting purposes only. In his master's degree thesis, Ernst Schillings suggested that in pilot tests, saline flushing proved to have the potential of an alternative to vacuum suction of the samples [44].

III. DESIGN AND DEVELOPMENT

The first and foremost prerequisite of the device is to be MRI safe or at least MRI conditional. Keeping this in view, all the parts are designed to be non-metallic or at least non-magnetic.

A. DESIGN REQUIREMENTS

A schematic of a teleoperated prostate biopsy system is shown in Figure 1. A multiple tissue sample collection and storage device (MTSCD) should be able to collect the core samples from the needle automatically and store them in a temporary storage space until the entire biopsy procedure is concluded. There were three basic considerations for the design of this device. Firstly, the device should be able to be teleoperated. Secondly, it should be able to collect multiple tissue samples during a biopsy session without needing the help of a medical staff member. Thirdly, it must be equipped with safe temporary storage with easy disinfection capability.

B. PROPOSED DESIGN

The proposed design of the device (MTSCD) is shown in Figure 2 [45], [46]. The basic principle is to use a piece of paper to collect the core sample. This piece of paper is rolled over two pulleys. When the pulleys rotate, the paper moves in the lateral direction. After removing the core sample, the needle is retracted backward and the core sample carrying slot of the needle is brought under the paper. Traditionally, a biopsy

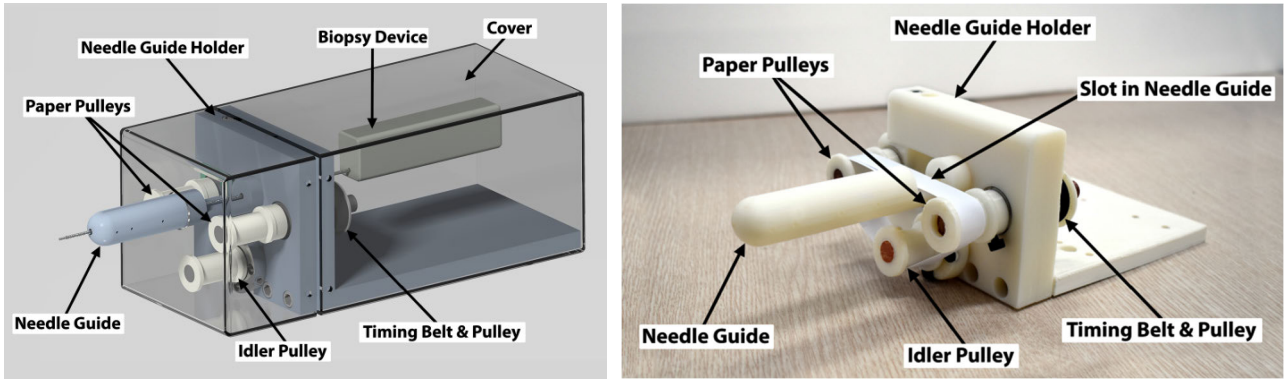

FIGURE 2. Multiple tissue sample collection device (MTSCD): 3D model (Left), 3D printed prototype (Right).

needle has two parts: an inner solid cylindrical shaped rod or Stylet and an outer tube or cannula. The cannula is retracted backward so that the tissue sample is exposed. The paper then starts moving in a lateral direction and thereby sweeps the tissue off the stylet slot which then sticks to the paper. To protect this tissue from getting contaminated or smudged over other surfaces, another layer of paper is introduced just below the needle. When the tissue sample is stuck on the paper, the lower layer of paper covers it and protects it from the surface of the pulley or other contaminations. These paper pulleys are mounted over shafts and the shafts are fitted in a base frame called a ''needle guide holder (NGH)''. The NGH platform in Figure 2 is of tentative shape and is designed in an 'L' shape. The horizontal part of the NGH is designed to be used as a connecting point with the robotic manipulator. The length of this part is variable which can be adjusted according to the design of the manipulator. Figure 1 shows the NGH connected to a robotic manipulator and a biopsy needle taking a sample of the prostate while patient is in the prone position. NGH has another cylindrical shaped structure called a ''Needle Guide (NG)'' between the two pulleys. The needle guide has a round shape from the front and has a hole in the center in the axial direction. This NG acts as a guide to the needle as well as an anal probe. The distal end of NG will be inserted into the anal cavity of the patient. The biopsy needle passes through the axial hole of NG. A slot is cut in the NG to accommodate the paper sweeping motion. The needle will be brought back to an extent where the needle slot is in the paper slot of the NG. To make sure that both paper pulleys rotate synchronously, a set of timing belt and two pulleys are installed on the proximal face of the NGH vertical part. To adjust the tension in the timing belt, one of the shafts is designed to have a variable position in the lateral direction. This shaft can move towards or away from other shaft and can be fixed with the help of a screw at a position where the tension in the belt has a desired value. Torque is supplied to the fixed pulley, which is visible in Figure 2, and is responsible for actuating the whole device. To control the tension in the paper layers, a similar approach was adopted. A third pulley with a variable position called an idler pulley was introduced. This pulley is below the NG and can move towards or away from NG vertically. Its position can also be fixed with the screws on its platform. It is to be clear that no biopsy device or manipulator is part of the design presented. In Figure 2(left) a transparent cover is shown encapsulating the whole device. This is a tentative design of the cover which is there to help protect the device from contamination. Cover shape and opacity is not necessarily as shown in Figure 2(left).

C. ACTUATION

Since the device will be working in an MRI environment, the actuation method must be MRI compatible as well. For this device, a piezoelectrically operated motor ''PSM60N-E2T'' by Piezo Sonic, Japan, will be used [47]. This motor has a maximum speed up to 120 rpm with a maximum torque of 1.2 Nm which is more than enough considering the device requires a very small amount of speed and torque. The motor has a built-in MRI conditional optical quadrature type rotary encoder with a resolution of 2000 pulses/rotation and 0.045° positioning accuracy.

D. WORKING OF THE DEVICE

The working of the device is explained in Figure 3. Initially, the automatic biopsy needle goes inside the patient's body to cut the core sample. Once the sample is transected successfully, the needle will be brought back using the robotic manipulator. The needle will move backward to an extent that the needle slot carrying the tissue sample is between the paper layers. It is made sure that the needle goes through the paper layers, i.e., one layer of paper is above and the other is below the needle. Please note that in Figure 3, the gap between two papers is exaggerated for the sake of understanding. Once the needle is in the desired position, the cannula is retracted, and tissue gets exposed to the paper. Till this point, every motion is actuated by the manipulator, or the biopsy needle and MTSCD has not been actuated yet. Once the tissue is exposed and ready to be collected, MTSCD is actuated. Pulleys start rotating and paper moves in the lateral direction. The tissue sample is swept off the needle slot and sticks to the paper surface. As soon as it moves away from the needle, the paper

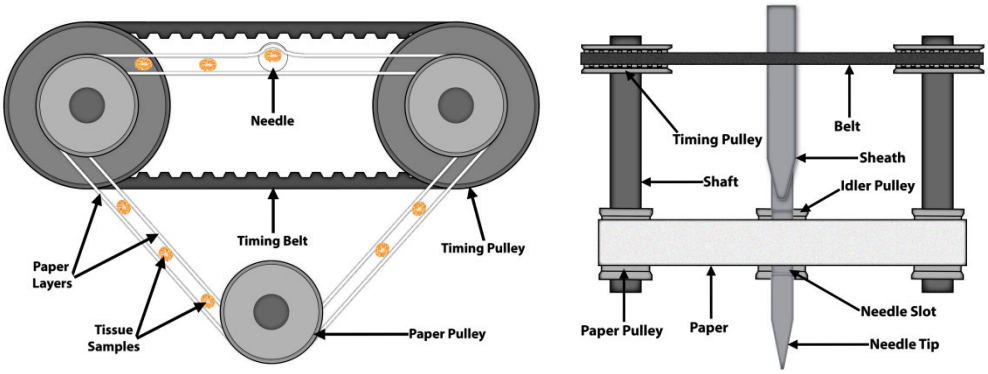

FIGURE 3. Schematic of working principle of MTSCD: front view (Left), top view (Right).

below the needle covers it and makes it secure between two layers of paper. The paper will stop moving after the current tissue sample is at a safe distance and the device will be ready to collect another sample. The cannula will move forward to cover the stylet and the needle will advance to take the next sample. Considering the length of the paper, the device will be able to collect 8-12 samples without changing the collecting paper. In one prostate biopsy session, the usually required number of core samples is 6-14 [48]. If in some cases more than 10 samples are needed to be collected, the paper gets up to full capacity and cannot collect any more samples, reloading of the paper is a very simple a quick task. All the paper pulleys can be removed by loosening a fixing screw that binds them with their respective shafts. Similarly, new pulleys carrying the paper can be loaded along with the paper and the fixing screw be tightened afterward. The position of the third pulley (idler pulley) should be adjusted before and after the loading process so that the paper does not tear up during the loading and unloading process.

Paper inelasticity does present a challenge in maintaining paper and belt tension. However, belt tension is maintained by moving the shaft laterally and it is prefixed before loading the paper. To adjust the paper tension, the motion of the idler pulley is used. So, tensions are adjusted in sequence which makes it manageable.

IV. EXPERIMENTS

Three types of experiments are discussed in this section. Firstly, a device performance evaluation test is performed in which sampling of the device is compared with manual sampling. Then, optimization of the device is done by changing the value of various parameters. A test is performed inside the MRI bore to check the MRI compatibility of the device.

A. DEVICE PERFORMANCE

A pilot test was performed to check the performance and feasibility of the device. As our team is currently working on the automatic biopsy needle, a commercially available manual biopsy needle "ACECUT" by TSK Laboratories, Japan was used to cut the samples from pork meat [49]. Eight samples were collected from the device manually i.e., by hand using a pre-weighed piece of paper and then weighed along with the paper. After subtracting the pre-recorded weight of the paper, tissue weight was noted. Using the same biopsy needle, the same number of samples were also collected by the MTSCD (Figure 4). A servo motor, XM540-W270 by Robotis Dynamixel was used as an actuator since the experiment is performed in a non-MR environment [50].

After the collection of samples, the paper was cut into pre-marked dimensions and weighed to make sure the weight of the paper piece is known to be subtracted. Results are shown in Figure 5. The average weight of the samples collected by the device was 3.93 mg with a standard deviation of 0.81 mg, while that of samples collected manually is 4.34 mg with a standard deviation of 0.44 mg. A statistical analysis was performed to see if the results of the two groups are significantly different. Since the samples are not mutually dependent, an independent two groups type T-test was performed. The summary of T-test is listed in Table 1 and Table 2. The calculated t-value of 1.263 is less than the critical value of 2.145 at the given confidence level and degrees of freedom. This indicates that the difference between the two samples is not significant. This experiment was performed using ordinary paper used for printing in daily use. Another experiment was performed using a smooth paper with a less porous and smooth surface finish to reduce the moisture absorption by the paper. A total of ten samples were collected for each group (manual and device sampling). The average weight of the samples collected by the device was 3.33 mg with a standard deviation of 0.39 mg, while that of samples collected manually is 3.38 mg with a standard deviation of 0.66 mg. A t-test was performed for this experiment as well. The summary of this t-test is listed in Table 1 and Table 2 as well. The calculated t-value of 0.2053 is less than the critical value of 2.101 at the given confidence level and degrees of freedom. This indicates that the difference between these data groups is not significant as well. Mean values for the smooth paper are closer to each other than the values for the ordinary paper. This appears to be due to the reduction in moisture absorption by smooth paper and eventually drying of the tissue samples. It may be noted that the average weight of collected tissues with ordinary paper and smooth paper are different in both

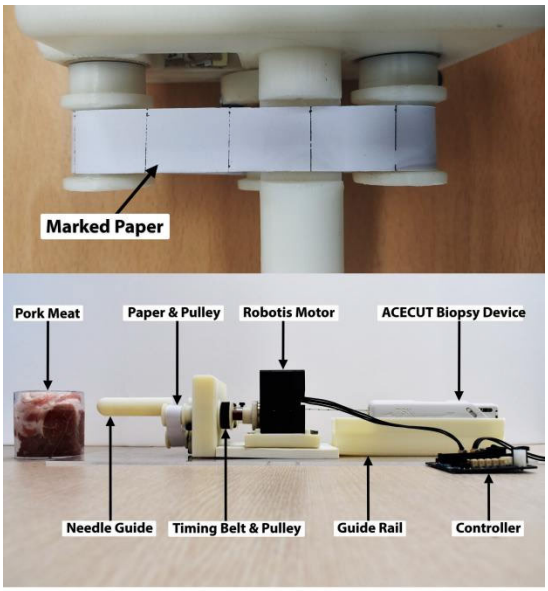

(a)

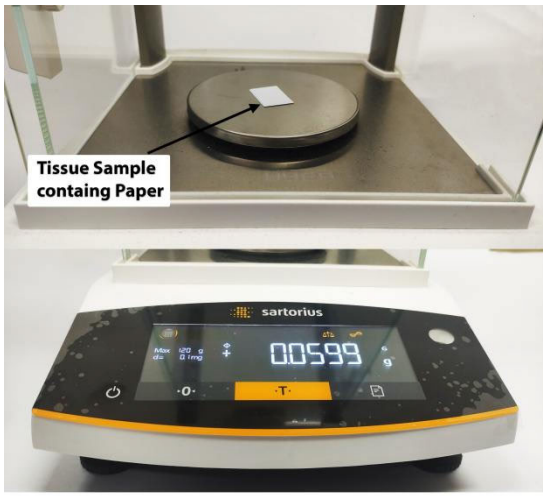

(b)

FIGURE 4. Device sampling performance evaluation: (a) Sampling configuration (b) Weighing of Tissue on a scale with a resolution of 0.1mg.

manual and device cases. This is due to the use of different meat and tissue nature for each paper resulting in different average sampling weights.

It takes approximately 12 minutes to collect the aforementioned number of samples by the devices. This time may be increased if the required time by the manipulator is added. Until the sampling process is concluded, previously collected samples cannot be moved to a formalin solution container for curing. The delay in tissue fixation may cause changes in the tissue samples which could be critical in diagnosis. Jackson et al. performed experiments to see the protein alterations in prostates of a rat and a beagle due to delayed freezing of the samples. Results showed that a short delay of up to 30 minutes showed no significant alterations [51]. However, as time increased the alterations increased significantly. Khoury et al. also performed experiments with breast cancer samples to see

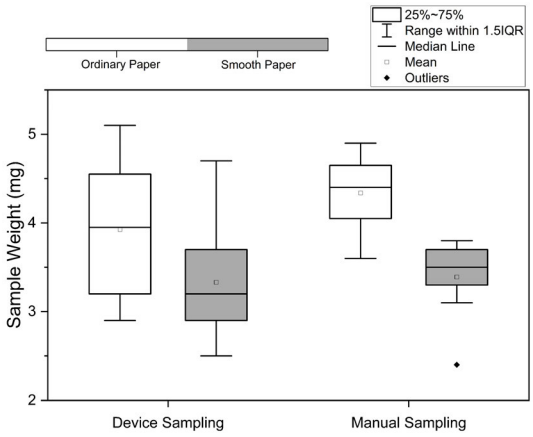

FIGURE 5. Comparison of MTSCD sampling and manual sampling.

the effects of delayed formalin fixation on the biomarkers in breast cancer. Results suggested that a delay of up to 1 hour did not affect the biomarkers significantly [52].

B. OPTIMIZATION EXPERIMENTS

Pilot tests were performed to test the workability of the device. To improve the sampling performance, three different experiments were also performed to optimize the performance of MTSCD. It can be noticed that the more the tension in the paper, the higher the pressure on the tissue exerted by the paper surface, resulting in more effective sample collection. But excessive pressure may also result in the distortion of the sample. To check the optimized value of tension in the paper, an experiment was performed with varying tensions. The experimental setup is shown in Figure 6. A load testing machine, which is a combination of a push-pull force gauge (HF-1 Set, JISC, Japan) and an automatic stand (a JSV-H1000-LM, JISC, Japan), was used in this experiment [53]. MTSCD was inverted such that the idler paper pulley is above the two main paper pulleys and fixed on the base of JSV-H1000. The idler pulley was connected with the force gauge end of HF-1. Force gauge can move upwards at very slow speed and the force on the gauge can be recorded on the display screen. As the force gauge moves upwards and the idler pulley goes with it, the tension in the paper is increased which is directly proportional to the force on the idler pulley. Seven samples were collected for five different force values ranging from 400gF to 800gF with an increment of 100gF. To evaluate the results, pictures of the needle slot were taken after the tissue sample have successfully been collected by MTSCD. These images were then converted into black & white images. In these black & white images, black represents the background surface of the needle slot, and white represents the residual tissues. The same commercially available manual biopsy needle "ACECUT" by TSK Laboratories, Japan as mentioned earlier in the text was used to cut the samples from pork meat. To take the microscopic images of the needle slot, a digital microscopic camera Dino Lite Edge by AnMo Electronics Corporation, Taiwan was used [54].

TABLE 1. Device and manual sampling characteristics.

Paper Type	Group	N	Mean	Std Deviation	Std. Error Mean
Ordinary Paper	Manual	8	4.33	0.44	0.16
	Device	8	3.92	0.81	0.29
Smooth Paper	Manual	10	3.38	0.39	0.13
	Device	10	3.33	0.66	0.21

TABLE 2. Independent samples T-test summary.

Group	F	Significance	t	df	Sig. (2 tailed)	Mean Difference	95% Confidence Interval of the Difference	
							Lower	**Upper**
Ordinary Paper	3.3489	0.0886	1.263	14	0.4132	-0.4125	-1.1131	0.2881
Smooth paper	0.4048	0.5348	0.2053	18	0.8396	-0.050	-0.562	0.462

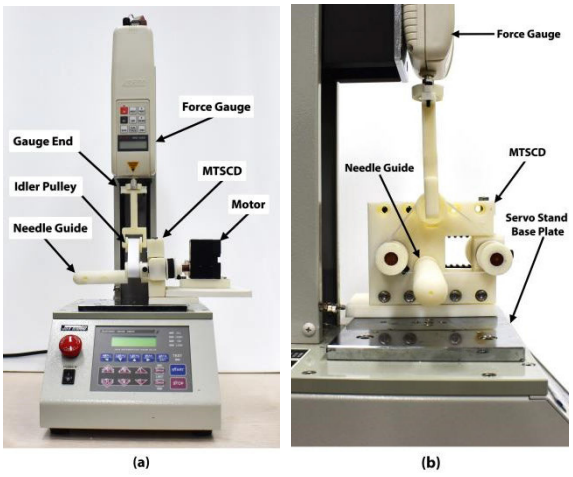

FIGURE 6. Parameters optimization experimental setup: (a) Side View (b) Front View.

The aforementioned greyscale images were later analyzed using OpenCV library in Python. ''Thresholding'' was utilized to convert the black & white images into absolute binary color images. OpenCV detected white regions as contours and calculated their area with respect to the total area of the image. This ratio represents the amount of residual tissue left on the needle after sample collection. Raw images taken by the microscopic camera and binary images are shown in Figure 7.

During this experiment, a width of the paper was introduced as another optimization variable. The needle slot had a length of 16mm, so three widths of paper were used from 15mm to 17mm with increments of 1mm. Hence a total number of 105 samples were collected in this experiment.

The third optimization variable was the speed of paper. The faster the speed of the motor, the faster the paper will move. So, to see the effect of the speed of the paper, three different speeds of the motor ranging from 5rpm to 15rpm with an increment of 5rpm were incorporated in the experiment. The corresponding speeds of the paper are 1.5 mm/sec, 3.0 mm/sec, and 4.5 mm/sec. Seven samples were taken for each value of the speed and results were averaged and evaluated in the same way as described earlier for the former experiments.

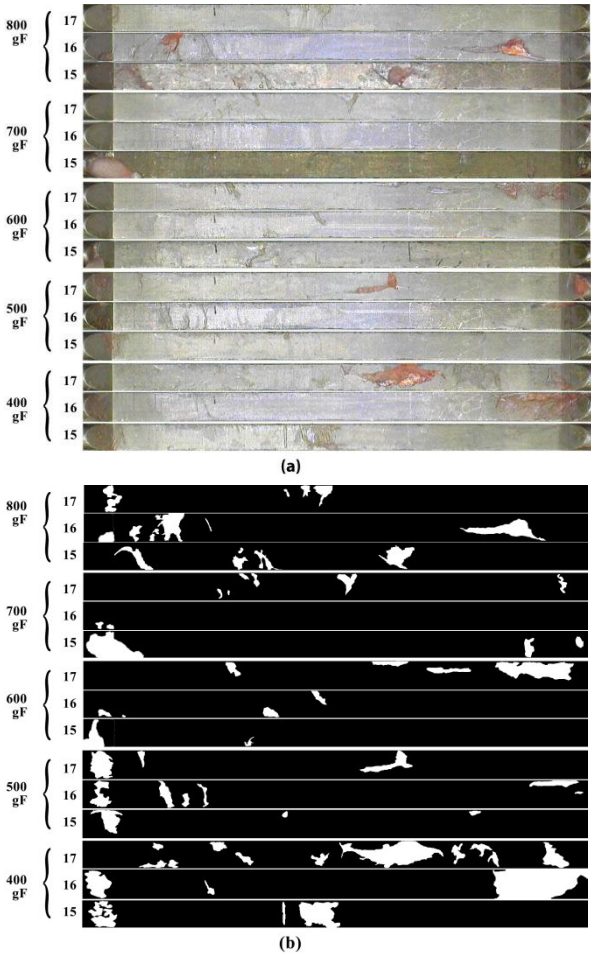

FIGURE 7. Tissue samples collected during optimization experiment under different forces and with different widths of paper: (a) Microscopic photographs of residual tissue on surface of needle slot after tissue collection (b) Binary images acquired from images in (a).

C. RESULTS

Seven samples were collected for each paper width for each force value and an average was taken. Figure 8(a) shows the results of the experiment where the average area covered by residual tissue is plotted against force values and paper widths. It is clear from the results that 600-700gF results in the lowest residual tissue-to-needle area ratio. A lower force or lower tension in the paper makes the paper wrinkled and it

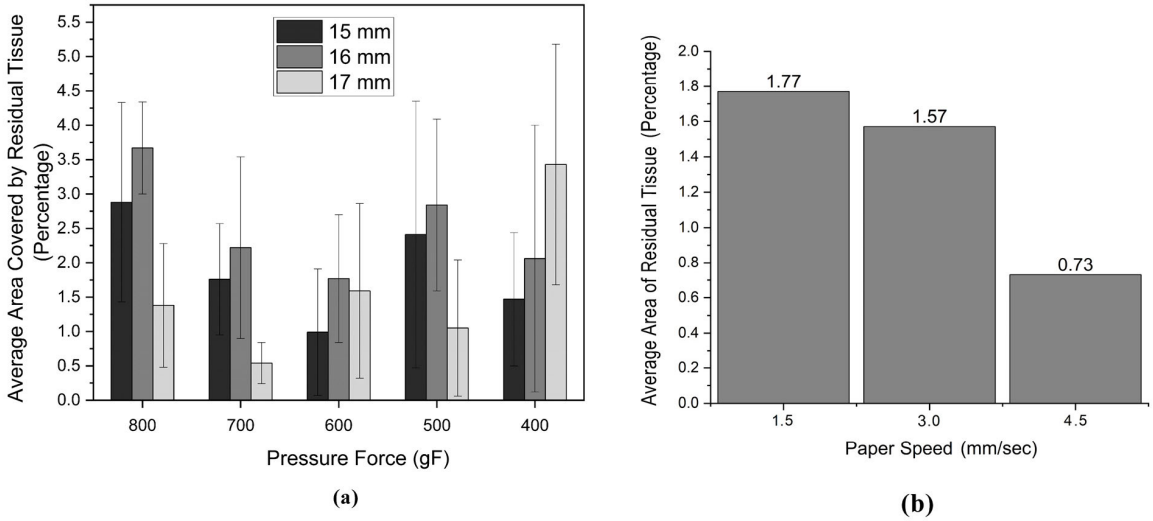

FIGURE 8. Optimization Results: (a) Residual tissue percentage plotted against pressure force for different widths of paper (b) Residual tissue percentage plotted against speed of the paper.

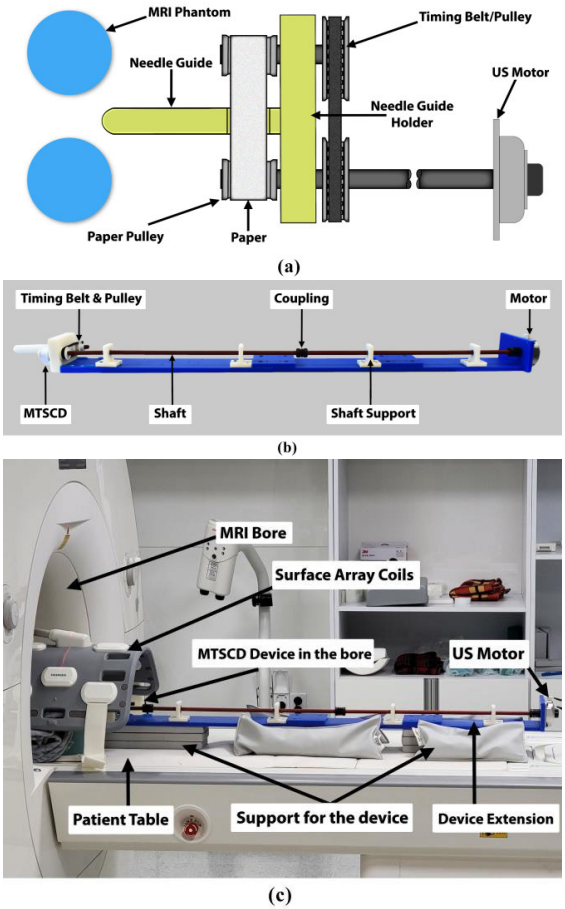

FIGURE 9. MRI compatibility evaluation Test: (a) Schematic of test configuration (b) Actual prototype to be placed in MRI system for test (c) Prototype placed in MRI bore under surface array coils.

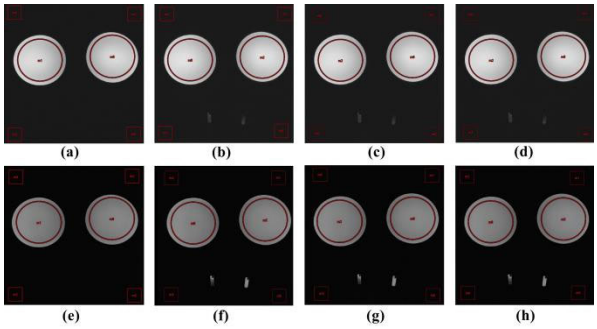

FIGURE 10. MRI scans: (a) ,(e) Phantom only, (b), (f) MTSCD placed in the bore with power off (c), (g) MTSCD placed in the bore with power on (d),(h) MTSCD placed in the bore while motor is operational. The upper image series (a)-(d) is T1 weighted while the lower image series (e)-(d) is T2 weighted.

could not touch the tissue sample effectively to sweep it off. Force higher than 700 gF means too much pressure on the tissue by paper which breaks the tissue into multiple pieces, and it gets smudged to the needle surface or paper. Paper with a width of 17 mm results in the lowest amount of residual tissue. The needle slot length is 16 mm, the collected tissue could have the same or smaller length. Thus, a 17 mm-wide paper provides an extra 1 mm width to make sure the whole length of the tissue gets in touch with the paper. It can also be noted that 17 mm width has better results for most of the force values.

Figure 8(b) shows the results of speed optimization experiments. The motor speed of 15 rpm results in the lowest residual tissue. At lower speeds, tissue sample experience pressure by the paper for longer time, which could break the tissue into smaller pieces resulting in a greater amount of residue. As the speed increases the contact time between the paper and the tissue sample is decreased and lateral force on the tissue is increased which helps the tissue not to break and stick with the paper as one piece.

Statistical Analyses were conducted to see if the results attained in previous tests were significantly different. A two-way ANOVA test for pressure force and size of the paper

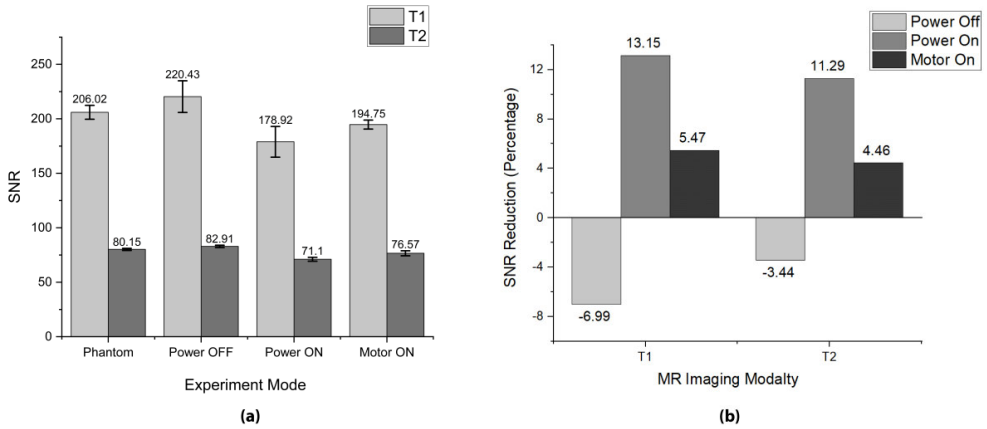

FIGURE 11. MRI compatibility evaluation test results: (a) SNR plotted for T1 and T2 imaging modalities against 04 testing configurations (b) SNR reduction in percentage plotted against T1 and T2 imaging modalities for 03 testing configurations.

was done. The F statistic for force is 3.12 with p-value of 0.018 which is higher than the critical F-value of 2.47 which means the results are significantly different. F-statistic for paper size is 4.21 with p-value of 0.018 which is higher than the critical F-value of 3.10, so size variance also results in significantly different results. Interaction of both force and paper size also has F-value (2.98) higher than F-critical (2.02) with the p-value of 0.005 and rejects the null hypothesis.

In the case of speed, one-way ANOVA results in F-value (1.52) less than critical F-value (2.59) with p-value of 0.222 which does not reject the null hypothesis and shows that speed does not have any significant effect on the results.

D. MRI COMPATIBILITY TESTS

As described earlier, a piezoelectric motor "PSM60N-E2T" by PiezoSonic, Japan, is used to actuate the MTSCD [25]. To check the MRI compatibility of the device, an experiment was performed in the MRI environment. The device was operated in the MRI room and noise produced by the system was compared by calculating the Signal-to-Noise ratio (SNR) reduction. A 3T MR scanner "Magnetom Skyra" and the flexible 18-ch body coil from Siemens, Germany were used to scan the images [55]. Experimental schematic and actual configurations are shown in Figure 9. The motor was installed 1100mm away from the device and a long shaft was used to deliver the torque to the device. In the first session (C1), MR system recorded the T1 and T2 weighted images of a pair of identical cylindrical MR phantoms (Siemens, Ø = 12cm, h = 18cm, 1900ml, per 1000g H_2O: 3.75g $NiSO_4$ x $6H_2O$ + 5g NaCl) only without the presence of MTSCD using FLASH (Fast Low Angle Shot) and TSE (Turbo Spin Echo) sequences respectively. The parameters of each sequence were as follows: FLASH(TR/TE = 540/2.84 msec, FOV(Field Of View) = 320 × 320 mm^2, slice thickness = 2 mm, matrix size = 320 × 320, acquisition time = 3 min 7 sec) and FSE(TR/TE = 9000/93 msec, FOV = 320 × 320 mm^2, slice thickness = 2 mm, matrix size = 320 × 320, acquisition time = 8 min 44 sec). Then, MTSCD was placed inside the bore and T1 and T2 weighted images were recorded. For the second session (C2), MTSCD was placed in the MRI bore and images were obtained without turning the power of the motor ON. In the third (C3) session, the setup was the same as of previous one, but the power was turned on. In the fourth and last session (C4), the motor was turned ON and images were obtained while the device was in operation. For all of the sessions, two types of imaging modalities (T1 and T2) were used. Images obtained are shown in Figure 10. The upper row shows the images for T1 modality while lower row shows the images for T2 modality. To calculate the SNR NEMA method 4 was used [56]. The signal value used was the average region of interest (ROI) area comprising 75% of the signal producing region of the image which can be seen as two circles. Four rectangular ROIs were drawn outside the phantom and away from any object to make sure they encompass the background region. Standard deviations of the noise region were averaged and divided by 0.66 Rician distribution correction factor to obtain the total image noise. SNR was then calculated as a ratio of average signal to average noise. For all eight cases, a total of 120 images (15 for each case) were used for SNR calculation. SNR was averaged over all 15 images of a series. For both T1 and T2 imaging, maximum SNR is noticed in the case C2 which is 220.43 ± 14.53 and 82.91 ± 1.12. SNR for each case is shown in Figure 11(a). SNR reduction for three cases (C2-C4) as compared to the case C1 has been shown as percentage in Figure 11(b). Maximum SNR reduction is noted in case C3 with device power ON which is 13.15% for T1 imaging while 11.29% in T2 imaging.

A one-way ANOVA was performed to see if the SNR differences between the three experimental modes are significant. For T1 images, F-value was 34.54 with p-value less than 0.001 which is greater than critical F-value 3.22 so null hypothesis is rejected, and the differences are significant. For T2 images, F-value was 151.05 with p-value less than 0.001 which is greater than critical F-value 3.22 which means the sample groups are significantly different.

V. CONCLUSION

A one-degree-of-freedom multiple tissue sample collection device is proposed in this paper which can receive multiple core samples from a biopsy device during a prostate biopsy. It also can store 8∼12 samples temporarily. The device works on the principle of a moving paper. The paper wipes the tissue sample off while sliding over it and stores it between two layers of paper. The pilot test consists of a comparison between the performance of the device and manual sampling using a paper. Results are sufficiently comparable. Further experiments were performed to optimize the tension in the paper, speed of the paper, and width of the paper to maximize the performance. Results are evaluated by a graphic analysis of the residual tissue quantity on the needle.

MRI compatibility evaluation tests of the device have also been performed. A piezoelectric motor is used to actuate the device in MRI room. Of all three configurations including Power off, Power turned on, and motor being operational, the maximum SNR reduction is found to be just 13.15% for T1 modality and 11.29% for T2 modality. Song et. al demonstrated a 44% SNR drop during the operation of the ultrasound motors for their motorized prostate biopsy guide template [57]. Su et. al reported a 19.8% SNR drop during the motor operation of their MRI-guided prostate percutaneous therapy system [39]. Krieger et. al reported a 40-60% SNR drop during the motor ON case for their MRI-compatible robotic system for prostate interventions [58]. These systems are MRI conditional. Our 1-DOF component designed for multiple tissue sample collection exhibits an SNR drop comparable to the studies reported by the groups and can be categorized as MRI conditional as well.

Although the device has been designed for a transrectal prostate biopsy, it has the potential to be modified and be used in other soft tissue biopsy procedures as well. For example, if the shape of the needle guide is altered according to the manipulator requirements, the device can be used in breast biopsy as well.

Several robotic systems have already been developed by several research teams for MRI guided prostate interventions [29], [30], [31], [32], [33], [34], [35], [36], [37], [38], [39], [40], [41], [42], [43]. Various biopsy devices have also been developed and are commercially available. Development of a multiple tissue sample collection device could be the final step towards the complete teleoperation of the MRI guided in-bore prostate biopsy. This device could not only decrease the procedure time significantly but could also immensely increase the efficiency and accuracy of the procedure.

VI. FUTURE WORK

This device is not a standalone system, and it requires an automatic biopsy needle which is capable of reloading and shooting itself as well as exposing the tissue at the required location of the MTSCD. Furthermore, a robotic manipulator with the ability of teleoperation, to orient the biopsy needle and support the MTSCD, is also an essential requirement of the system. Both of the aforementioned components are being developed by our team. In the future, it is planned to integrate all three parts into one system and test it within the MR environment. In addition, there are plans to conduct additional tests in the future to assess the device's image quality and ensure its safe usage in the MRI room. Moreover, pathological analysis will be performed to assess how the rolling between the paper affects the tissue sample's integrity and its usability in the lab.

REFERENCES

[1] H. Sung, J. Ferlay, R. L. Siegel, M. Laversanne, I. Soerjomataram, A. Jemal, and F. Bray, "Global cancer statistics 2020: GLOBOCAN estimates of incidence and mortality worldwide for 36 cancers in 185 countries," *CA, Cancer J. Clinicians*, vol. 71, no. 3, pp. 209–249, May 2021, doi: 10.3322/caac.21660.

[2] R. A. Smith, K. S. Andrews, D. Brooks, S. A. Fedewa, D. Manassaram-Baptiste, D. Saslow, and R. C. Wender, "Cancer screening in the United States, 2019: A review of current American cancer society guidelines and current issues in cancer screening," *CA, Cancer J. Clinicians*, vol. 69, no. 3, pp. 184–210, May 2019, doi: 10.3322/caac.21557.

[3] W. J. Catalona, J. P. Richie, F. R. Ahmann, A. H. M'Liss, P. T. Scardino, R. C. Flanigan, and J. B. Dekernion, "Comparison of digital rectal examination and serum prostate specific antigen in the early detection of prostate cancer: Results of a multicenter clinical trial of 6,630 men," *J. Urol.*, vol. 151, no. 5, pp. 1283–1290, May 1994, doi: 10.1016/S0022-5347(17)35233-3.

[4] J. H. Yacoub, S. Verma, J. S. Moulton, S. Eggener, and A. Oto, "Imaging-guided prostate biopsy: Conventional and emerging techniques," *RadioGraphics*, vol. 32, no. 3, pp. 819–837, May 2012, doi: 10.1148/rg.323115053.

[5] C. Tonry, S. Finn, J. Armstrong, and S. R. Pennington, "Clinical proteomics for prostate cancer: Understanding prostate cancer pathology and protein biomarkers for improved disease management," *Clin. Proteomics*, vol. 17, no. 1, p. 41, Dec. 2020, doi: 10.1186/s12014-020-09305-7.

[6] A. Thomson, M. Li, J. Grummet, and S. Sengupta, "Transperineal prostate biopsy: A review of technique," *Transl. Androl. Urol.*, vol. 9, no. 6, pp. 3009–3017, Dec. 2020, doi: 10.21037/tau.2019.12.40.

[7] J. Grummet, L. Pepdjonovic, S. Huang, E. Anderson, and B. Hadaschik, "Transperineal vs. transrectal biopsy in MRI targeting," *Transl. Androl. Urol.*, vol. 6, no. 3, pp. 368–375, Jun. 2017, doi: 10.21037/tau.2017.03.58.

[8] N. Lawrentschuk, M. A. Haider, N. Daljeet, A. Evans, A. Toi, A. Finelli, J. Trachtenberg, A. Zlotta, and N. Fleshner, "'Prostatic evasive anterior tumours': The role of magnetic resonance imaging," *BJU Int.*, vol. 105, no. 9, pp. 1231–1236, May 2010, doi: 10.1111/j.1464-410X.2009.08938.x.

[9] F. K.-H. Chun, T. Steuber, A. Erbersdobler, E. Currlin, J. Walz, T. Schlomm, A. Haese, H. Heinzer, M. McCormack, H. Huland, M. Graefen, and P. I. Karakiewicz, "Development and internal validation of a nomogram predicting the probability of prostate cancer Gleason sum upgrading between biopsy and radical prostatectomy pathology," *Eur. Urol.*, vol. 49, no. 5, pp. 820–826, May 2006, doi: 10.1016/j.eururo.2005.11.007.

[10] C. J. Das, A. Razik, A. Netaji, and S. Verma, "Prostate MRI–TRUS fusion biopsy: A review of the state of the art procedure," *Abdominal Radiol.*, vol. 45, no. 7, pp. 2176–2183, Jul. 2020, doi: 10.1007/s00261-019-02391-8.

[11] S. Verma, P. L. Choyke, S. C. Eberhardt, A. Oto, C. M. Tempany, B. Turkbey, and A. B. Rosenkrantz, "The current state of MR imaging–targeted biopsy techniques for detection of prostate cancer," *Radiology*, vol. 285, no. 2, pp. 343–356, Nov. 2017, doi: 10.1148/radiol.2017161684.

[12] I. G. Schoots, M. J. Roobol, D. Nieboer, C. H. Bangma, E. W. Steyerberg, and M. G. M. Hunink, "Magnetic resonance imaging–targeted biopsy may enhance the diagnostic accuracy of significant prostate cancer detection compared to standard transrectal ultrasound-guided biopsy: A systematic review and meta-analysis," *Eur. Urol.*, vol. 68, no. 3, pp. 438–450, Sep. 2015, doi: 10.1016/j.eururo.2014.11.037.

[13] J. Kam, Y. Yuminaga, R. Kim, K. Aluwihare, F. Macneil, R. Ouyang, S. Ruthven, and M. Louie-Johnsun, "Does magnetic resonance imaging–guided biopsy improve prostate cancer detection? A comparison of systematic, cognitive fusion and ultrasound fusion prostate biopsy," *Prostate Int.*, vol. 6, no. 3, pp. 88–93, Sep. 2018, doi: 10.1016/j.prnil.2017.10.003.

[14] M. van der Leest, E. Cornel, B. Israël, R. Hendriks, A. R. Padhani, M. Hoogenboom, P. Zamecnik, D. Bakker, A. Y. Setiasti, J. Veltman, H. van den Hout, H. van der Lelij, I. van Oort, S. Klaver, F. Debruyne, M. Sedelaar, G. Hannink, M. Rovers, C. Hulsbergen-van de Kaa, and J. O. Barentsz, "Head-to-head comparison of transrectal ultrasound-guided prostate biopsy versus multiparametric prostate resonance imaging with subsequent magnetic resonance-guided biopsy in biopsy-naïve men with elevated prostate-specific antigen: A large prospective multicenter clinical study," *Eur. Urol.*, vol. 75, no. 4, pp. 570–578, Apr. 2019, doi: 10.1016/j.eururo.2018.11.023.

[15] M. M. Siddiqui, S. Rais-Bahrami, H. Truong, L. Stamatakis, S. Vourganti, J. Nix, A. N. Hoang, A. Walton-Diaz, B. Shuch, M. Weintraub, J. Kruecker, H. Amalou, B. Turkbey, M. J. Merino, P. L. Choyke, B. J. Wood, and P. A. Pinto, "Magnetic resonance imaging/ultrasound–fusion biopsy significantly upgrades prostate cancer versus systematic 12-core transrectal ultrasound biopsy," *Eur. Urol.*, vol. 64, no. 5, pp. 713–719, Nov. 2013, doi: 10.1016/j.eururo.2013.05.059.

[16] J. J. Fütterer and J. O. Barentsz, "MRI-guided and robotic-assisted prostate biopsy," *Current Opinion Urol.*, vol. 22, no. 4, pp. 316–319, Jul. 2012, doi: 10.1097/MOU.0b013e328354833c.

[17] A. Shukla-Dave and H. Hricak, "Role of MRI in prostate cancer detection," *NMR Biomed.*, vol. 27, no. 1, pp. 16–24, Jan. 2014, doi: 10.1002/nbm.2934.

[18] B. Turkbey and P. L. Choyke, "Multiparametric MRI and prostate cancer diagnosis and risk stratification," *Current Opinion Urol.*, vol. 22, no. 4, pp. 310–315, Jul. 2012, doi: 10.1097/MOU.0b013e32835481c2.

[19] D. G. Engehausen, K. Engelhard, S. A. Schwab, M. Uder, S. Wach, B. Wullich, and F. S. Krause, "Magnetic resonance image-guided biopsies with a high detection rate of prostate cancer," *Sci. World J.*, vol. 2012, pp. 1–6, Jan. 2012, doi: 10.1100/2012/975971.

[20] C. M. Moore, N. L. Robertson, N. Arsanious, T. Middleton, A. Villers, L. Klotz, S. S. Taneja, and M. Emberton, "Image-guided prostate biopsy using magnetic resonance imaging–derived targets: A systematic review," *Eur. Urol.*, vol. 63, no. 1, pp. 125–140, Jan. 2013, doi: 10.1016/j.eururo.2012.06.004.

[21] T. Franiel, C. Stephan, A. Erbersdobler, E. Dietz, A. Maxeiner, N. Hell, A. Huppertz, K. Miller, R. Strecker, and B. Hamm, "Areas suspicious for prostate cancer: MR-guided biopsy in patients with at least one transrectal U.S.-guided biopsy with a negative finding-multiparametric MR imaging for detection and biopsy planning," *Genitourinary Imag.*, vol. 259, no. 1, p. 11, 2011.

[22] L. Lee and J. Pilcher, "The role of transrectal ultrasound and biopsy in the diagnosis and management of prostate cancer," *Imaging*, vol. 20, no. 2, pp. 122–130, Jun. 2008, doi: 10.1259/imaging/41490379.

[23] K. Engelhard, H. P. Hollenbach, B. Kiefer, A. Winkel, K. Goeb, and D. Engehausen, "Prostate biopsy in the supine position in a standard 1.5-T scanner under real time MR-imaging control using a MR-compatible endorectal biopsy device," *Eur. Radiol.*, vol. 16, no. 6, pp. 1237–1243, May 2006, doi: 10.1007/s00330-005-0100-6.

[24] T. Hambrock, D. M. Somford, C. Hoeks, S. A. W. Bouwense, H. Huisman, D. Yakar, I. M. van Oort, J. A. Witjes, J. J. Fütterer, and J. O. Barentsz, "Magnetic resonance imaging guided prostate biopsy in men with repeat negative biopsies and increased prostate specific antigen," *J. Urol.*, vol. 183, no. 2, pp. 520–528, Feb. 2010, doi: 10.1016/j.juro.2009.10.022.

[25] A. G. Anastasiadis, M. P. Lichy, U. Nagele, M. A. Kuczyk, A. S. Merseburger, J. Hennenlotter, S. Corvin, K.-D. Sievert, C. D. Claussen, A. Stenzl, and H.-P. Schlemmer, "MRI-guided biopsy of the prostate increases diagnostic performance in men with elevated or increasing PSA levels after previous negative TRUS biopsies," *Eur. Urol.*, vol. 50, no. 4, pp. 738–749, Oct. 2006, doi: 10.1016/j.eururo.2006.03.007.

[26] D. Beyersdorff, A. Winkel, B. Hamm, S. Lenk, S. A. Loening, and M. Taupitz, "MR imaging–guided prostate biopsy with a closed MR unit at 1.5 T: Initial results," *Radiology*, vol. 234, no. 2, pp. 576–581, Feb. 2005, doi: 10.1148/radiol.2342031887.

[27] O. Ruprecht, P. Weisser, B. Bodelle, H. Ackermann, and T. J. Vogl, "MRI of the prostate: Interobserver agreement compared with histopathologic outcome after radical prostatectomy," *Eur. J. Radiol.*, vol. 81, no. 3, pp. 456–460, Mar. 2012, doi: 10.1016/j.ejrad.2010.12.076.

[28] M. U. Farooq and S. Y. Ko, "A decade of MRI compatible robots: Systematic review," *IEEE Trans. Robot.*, vol. 39, no. 2, pp. 862–884, Apr. 2023, doi: 10.1109/TRO.2022.3212626.

[29] F. G. Shellock, "Magnetic resonance safety update 2002: Implants and devices," *J. Magn. Reson. Imag.*, vol. 16, no. 5, pp. 485–496, Nov. 2002, doi: 10.1002/jmri.10196.

[30] S. Elayaperumal, M. R. Cutkosky, P. Renaud, and B. L. Daniel, "A passive parallel master–slave mechanism for magnetic resonance imaging-guided interventions," *J. Med. Devices*, vol. 9, no. 1, Mar. 2015, Art. no. 011008, doi: 10.1115/1.4028944.

[31] E. Mendoza and J. P. Whitney, "A testbed for haptic and magnetic resonance imaging-guided percutaneous needle biopsy," *IEEE Robot. Autom. Lett.*, vol. 4, no. 4, pp. 3177–3183, Oct. 2019, doi: 10.1109/LRA.2019.2925558.

[32] Y. Chen, A. Squires, R. Seifabadi, S. Xu, H. K. Agarwal, M. Bernardo, P. A. Pinto, P. Choyke, B. Wood, and Z. T. H. Tse, "Robotic system for MRI-guided focal laser ablation in the prostate," *IEEE/ASME Trans. Mechatronics*, vol. 22, no. 1, pp. 107–114, Feb. 2017, doi: 10.1109/TMECH.2016.2611570.

[33] R. Seifabadi, S.-E. Song, A. Krieger, N. B. Cho, J. Tokuda, G. Fichtinger, and I. Iordachita, "Robotic system for MRI-guided prostate biopsy: Feasibility of teleoperated needle insertion and ex vivo phantom study," *Int. J. Comput. Assist. Radiol. Surg.*, vol. 7, no. 2, pp. 181–190, Mar. 2012, doi: 10.1007/s11548-011-0598-9.

[34] S.-E. Song, N. B. Cho, G. Fischer, N. Hata, C. Tempany, G. Fichtinger, and I. Iordachita, "Development of a pneumatic robot for MRI-guided transperineal prostate biopsy and brachytherapy: New approaches," in *Proc. IEEE Int. Conf. Robot. Autom.*, May 2010, pp. 2580–2585, doi: 10.1109/ROBOT.2010.5509710.

[35] D. Stoianovici, A. Patriciu, D. Petrisor, D. Mazilu, and L. Kavoussi, "A new type of motor: Pneumatic step motor," *IEEE/ASME Trans. Mechatronics*, vol. 12, no. 1, pp. 98–106, Feb. 2007, doi: 10.1109/TMECH.2006.886258.

[36] D. Stoianovici, C. Kim, D. Petrisor, C. Jun, S. Lim, M. W. Ball, A. Ross, K. J. Macura, and M. E. Allaf, "MR safe robot, FDA clearance, safety and feasibility of prostate biopsy clinical trial," *IEEE/ASME Trans. Mechatronics*, vol. 22, no. 1, pp. 115–126, Feb. 2017, doi: 10.1109/TMECH.2016.2618362.

[37] S. Jiang, J. Guo, S. Liu, J. Liu, and J. Yang, "Kinematic analysis of a 5-DOF hybrid-driven MR compatible robot for minimally invasive prostatic interventions," *Robotica*, vol. 30, no. 7, pp. 1147–1156, Dec. 2012, doi: 10.1017/S0263574711001317.

[38] Y. Lin, Y. Shi, J. Zhang, F. Wang, W. Wu, and H. Sun, "Design and control of a piezoelectric actuated prostate intervention robotic system," in *Proc. 17th Int. Conf. Ubiquitous Robots (UR)*, Kyoto, Japan, Jun. 2020, pp. 175–180, doi: 10.1109/UR49135.2020.9144768.

[39] H. Su, W. Shang, G. Cole, G. Li, K. Harrington, A. Camilo, J. Tokuda, C. M. Tempany, N. Hata, and G. S. Fischer, "Piezoelectrically actuated robotic system for MRI-guided prostate percutaneous therapy," *IEEE/ASME Trans. Mechatronics*, vol. 20, no. 4, pp. 1920–1932, Aug. 2015, doi: 10.1109/TMECH.2014.2359413.

[40] P. Moreira, G. van de Steeg, T. Krabben, J. Zandman, E. E. G. Hekman, F. van der Heijden, R. Borra, and S. Misra, "The MIRIAM robot: A novel robotic system for MR-guided needle insertion in the prostate," *J. Med. Robot. Res.*, vol. 2, no. 4, Dec. 2017, Art. no. 1750006, doi: 10.1142/S2424905X17500064.

[41] J. A. Hibner and M. R. Ludzack, *(75) Inventors*. Mason, OH, USA: Shailendra K. Parihar, 2010, p. 32.

[42] S. C. Anderson, J. W. Vetter, and D. M. Brounstein, *(75) Inventors*. Los Altos, CA, USA: Mark J. Clifford, 2009, p. 33.

[43] R. S. Pesce, S. Cook, K. DiMatteo, K. Ranucci, and R. Boock, "Tissue extraction and collection device," U.S. Patent 2008/0 234 715 A1, Sep. 25, 2008.

[44] E. Schillings, "A biopsy system that can automatically sample and remove prostate biopsy samples," M.S thesis, Dept. Mech., Maritime Mater. Eng., Delft Univ. Technol., Delft, The Netherlands, 2019. [Online]. Available: http://resolver.tudelft.nl/uuid:5fd77c23-39a8-49de-ac6b-e968d38f7c61

[45] F. Anique, J. K. Jo, and S. Y. Ko, "Multiple tissue sample collection device for mri guided transrectal prostate biopsy: Preliminary study," in *Proc. IEEE Int. Conf. Robot. Biomimetics (ROBIO)*, Sanya, China, Dec. 2021, pp. 221–225, doi: 10.1109/ROBIO54168.2021.9739271.

[46] F. Anique, J. K. Jo, and S. Y. Ko, "Tension optimization in multiple tissue sample collection device for MRI-guided transrectal prostate biopsy: A preliminary work," in *Proc. IEEE Int. Conf. Robot. Biomimetics (ROBIO)*, Jeju, South Korea, Dec. 2021, pp. 455–458.

[47] Piezo Sonic. *2,000P/R Motor With Encoder PSM60N-E2T*. Accessed: Aug. 2, 2022. [Online]. Available: https://www.piezo-sonic.com/products/nonmagnetic/psm60n-e2t
[48] L. Nesrallah, A. Nesrallah, A. A. Antunes, K. R. Leite, and M. Srougi, "The role of extended prostate biopsy on prostate cancer detection rate: A study performed on the bench," *Int. Braz J.*, vol. 34, no. 5, pp. 563–571, Oct. 2008, doi: 10.1590/S1677-55382008000500004.
[49] TSK Laboratory. *ACECUT*. Japan. Accessed: Aug. 2, 2022. [Online]. Available: https://www.tsklab.co.jp/en/products/biopsy_needle/acecut.php
[50] ROBOTIS. *ROBOTIS E-Manual*. Accessed: Aug. 2, 2022. [Online]. Available: https://emanual.robotis.com/docs/en/dxl/x/xm540-w270/
[51] D. Jackson, R. A. Rowlinson, C. K. Eaton, J. A. Nickson, I. D. Wilson, J. D. Mills, R. W. Wilkinson, and R. P. Tonge, "Prostatic tissue protein alterations due to delayed time to freezing," *PROTEOMICS*, vol. 6, no. 13, pp. 3901–3908, Jul. 2006, doi: 10.1002/pmic.200500794.
[52] T. Khoury, S. Sait, H. Hwang, R. Chandrasekhar, G. Wilding, D. Tan, and S. Kulkarni, "Delay to formalin fixation effect on breast biomarkers," *Modern Pathol.*, vol. 22, no. 11, pp. 1457–1467, Nov. 2009, doi: 10.1038/modpathol.2009.117.
[53] *ALGOL*. Taiwan. Accessed: Aug. 2, 2022. [Online]. Available: https://www.algol.com.tw/en/product_description.php?PNo=26&Protype=product&CNo=43
[54] *Dino-Lite Digital Microscope*. Taiwan. Accessed: Aug. 2, 2022. [Online]. Available: https://www.dino-lite.com/products_detail.php?index_m1_id=9&index_m2_id=47&index_id=169
[55] *MAGNETOM Skyra—Siemens Healthineers*. Accessed: Aug. 2, 2022. [Online]. Available: https://www.siemens-healthineers.com/magnetic-resonance-imaging/3t-mri-scanner/magnetom-skyra
[56] F. L. Goerner and G. D. Clarke, "Measuring signal-to-noise ratio in partially parallel imaging MRI," *Med. Phys.*, vol. 38, no. 9, pp. 5049–5057, Aug. 2011, doi: 10.1118/1.3618730.
[57] S. Song, J. Tokuda, K. Tuncali, C. M. Tempany, E. Zhang, and N. Hata, "Development and preliminary evaluation of a motorized needle guide template for MRI-guided targeted prostate biopsy," *IEEE Trans. Biomed. Eng.*, vol. 60, no. 11, pp. 3019–3027, Nov. 2013, doi: 10.1109/TBME.2013.2240301.
[58] A. Krieger, S. Song, N. B. Cho, I. I. Iordachita, P. Guion, G. Fichtinger, and L. L. Whitcomb, "Development and evaluation of an actuated MRI-compatible robotic system for MRI-guided prostate intervention," *IEEE/ASME Trans. Mechatronics*, vol. 18, no. 1, pp. 273–284, Feb. 2013, doi: 10.1109/TMECH.2011.2163523.

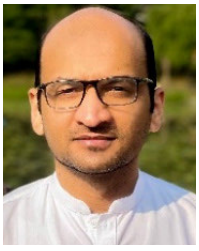

FARRUKH ANIQUE received the B.S. degree in mechanical engineering and the M.S. degree in nuclear power engineering from the Pakistan Institute of Engineering and Applied Sciences (PIEAS), Islamabad, Pakistan, in 2014 and 2016, respectively. He is currently pursuing the Ph.D. degree with the Department of Mechanical Engineering, Chonnam National University, Gwangju, Republic of Korea.

His research interests include surgical robots, medical devices, and flow and thermal simulations.

RONGRONG LIU received the B.S. degree in mechanical engineering from Wenzhou University, Wenzhou, China, in 2016, and the M.S. degree from the Department of Mechanical Engineering, Chonnam National University, Gwangju, Republic of Korea, where she is currently pursuing the Ph.D. degree.

Her research interests include medical robotics and intelligent control.

MUHAMMAD UMAR FAROOQ received the B.S. degree in mechanical engineering from the Pakistan Institute of Engineering and Applied Sciences (PIEAS), Islamabad, Pakistan, in 2015, and the M.S. and Ph.D. degrees in mechanical engineering from Chonnam National University, Republic of Korea, in 2017 and 2021, respectively.

He is currently a Postdoctoral Researcher with the Department of Industrial and Systems Engineering, Korea Advanced Institute of Science and Technology (KAIST), Daejeon, South Korea. His research interests include medical and surgical robots, autonomous mobile robots, industrial automation, and robot control and actuators.

SUNG SUK OH received the B.S. degree in electrical engineering from Kyungbook National University, Daegu, South Korea, in 2003, and the M.S. and Ph.D. degrees in biosystem engineering and electrical engineering from the Korea Advanced Institute of Science and Technology (KAIST), Daejeon, South Korea, in 2006 and 2014, respectively.

From 2012 to 2014, he was a Research Fellow with the Department of Radiology, University of Pennsylvania, USA; and a Postdoctoral Researcher in electrical engineering with Seoul National University, South Korea. He is currently a Senior Researcher with the Daegu–Gyeongbuk Medical Innovation Foundation (K-MEDI Hub), Daegu. His research interests include multi-modal medical imaging, image processing, and brain signal processing.

JUNG KI JO received the degree from the College of Medicine, Hanyang University, in 2005, and the Ph.D. degree from the Department of Urology, Graduate School of Medicine, Hanyang University, in 2016. He is an Associate Professor with the Department of Urology, Hanyang University College of Medicine. He is also a Chief of the HYUH Bio Convergence Medical Device Center. He is a specialist of uro-oncology, including prostate cancer, kidney cancer, and bladder cancer. His research interest includes medical robotics.

SEONG YOUNG KO (Member, IEEE) received the B.S., M.S., and Ph.D. degrees from the Department of Mechanical Engineering, Korea Advanced Institute of Science and Technology (KAIST), Daejeon, South Korea, in 2000, 2002, and 2008, respectively.

From 2009 to 2011, he was a Research Associate with the Mechatronics in Medicine Laboratory, Department of Mechanical Engineering, Imperial College London, U.K. Since October 2011, he has been an Assistant Professor/an Associate Professor with the School of Mechanical Engineering, Chonnam National University, Gwangju, South Korea, where he is currently a Professor. His research interests include medical robotics, human–robot interaction, and intelligent control.